Photo-catalytic activity of BiVO4 thin film electrodes for solar-driven water splitting

Citation Information:
Hernández S, Thalluri SM, Sacco A, Bensaid S, Saracco G, Russo N. Photo-catalytic activity of BiVO4 thin-film electrodes for solar-driven water splitting. Applied Catalysis A: General. 2015; DOI: 10.1016/j.apcata.2015.01.019.

G Model
APCATA-15211; No. of Pages 6
ARTICLE IN PRESS

Applied Catalysis A: General xxx (2015) xxx–xxx

Contents lists available at ScienceDirect

Applied Catalysis A: General

journal homepage: www.elsevier.com/locate/apcata

Photo-catalytic activity of $BiVO_4$ thin-film electrodes for solar-driven water splitting

Simelys Hernández [a,b], Sitaramanjaneya Mouli Thalluri [a], Adriano Sacco [b], Samir Bensaid [a], Guido Saracco [a], Nunzio Russo [a,*]

[a] Department of Applied Science and Technology, Politecnico di Torino, Corso Duca degli Abruzzi 24, 10129 Torino, Italy
[b] Center for Space Human Robotics (IIT@POLITO), Istituto Italiano di Tecnologia, C.so Trento 21, 10129 Torino, Italy

Graphical Abstract:

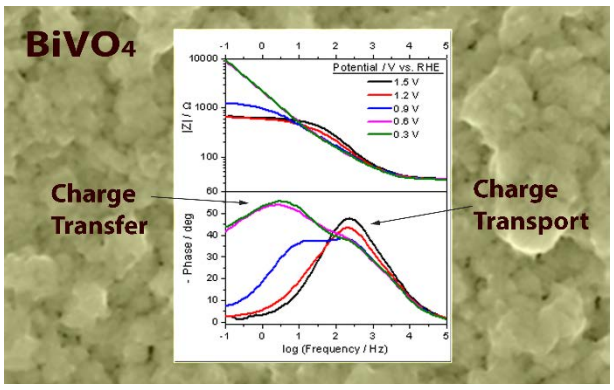

Photo-catalytic activity of $BiVO_4$ thin film electrodes for solar-driven water splitting

Simelys Hernández [a,b], Sitaramanjaneya Mouli Thalluri,[a] Adriano Sacco,[b] Samir Bensaid,[a] Guido Saracco,[a] Nunzio Russo [a,*]

[a] *Department of Applied Science and Technology, Politecnico di Torino, Corso Duca degli Abruzzi 24, 10129 Torino, Italy*

[b] *Center for Space Human Robotics (IIT@POLITO), Istituto Italiano di Tecnologia, C.so Trento 21, 10129, Torino, Italy*

**corresponding author: Tel: +39-011-0904710; E-mail:nunzio.russo@polito.it*

Abstract

There is an ever-increasing attention directed to the development of solar fuels by photo electrochemical water splitting, given the inexhaustible availability of solar energy. The water oxidation half-reaction is a critical step for the overall water splitting reaction, and the development of suitable photoanodes is therefore required. The present research work focuses on bismuth vanadate thin films' deposition on FTO glass electrodes, through the dip coating technique, and discusses the influence of the film preparation technique on the electrodes photo-electrochemical performance.

The bismuth vanadate thin films were synthesized with thicknesses ranging from 60 to 210 nm, depending on a number of dip coatings from 2 to 15. The structural and optical characterization of the films showed that monoclinic scheelite-type phase was obtained in all samples, with crystal sizes ranging from 24 to 65 nm, at increasing film thicknesses, and corresponding band gaps between 2.55 and 2.35 eV. A maximum photo-current density of about 0.57 $mA.cm^{-2}$ at 1.23 V vs. RHE under sunlight illumination was obtained for an electrode thickness of 160 nm. The electrochemical impedance spectroscopy elucidated the transport mechanisms occurring at the electrolyte-electrode interface, as well as inside the film. The estimation of the equivalent circuit parameters showed that an increasing film thickness decreased the resistance associated to the charge transfer between the electrolyte and the electrode (from 1100 to 450 Ω, from 60 to 160 nm layer thickness, respectively), given the higher number of active sites involved in the reaction. However, excessive film thicknesses increase the probability of charge recombination within the film and, in the specific case here investigated, can also be associated to film imperfections arising from several deposition-calcination cycles, which further act as traps. These concurring phenomena are of high relevance to isolate the rate-determining step of the water oxidation half-reaction, in the perspective of an optimization of bismuth vanadate film coating on FTO to obtain photo anodes.

Keywords: $BiVO_4$, dip-coating, thin film, water splitting, electrochemical impedance spectroscopy, photocatalyst.

Applied Catalysis A: General xxx (2015) xxx–xxx
DOI: 10.1016/j.apcata.2015.01.019

1. Introduction

The most promising technology for the production of hydrogen from renewable energy sources is photo-electrochemical water splitting exploiting solar light [1, 2]. However, the greatest challenge of this technology is that anodic electrodes are needed to overcome the high over-potential required to perform the water oxidation four-electron reaction, which is responsible for the slow kinetics of such a photo-electrochemical system [3]. There is an ever increasing need to develop efficient and robust light harvesters, water oxidation catalysts and photo-catalysts in order to develop a commercially viable photo-electrochemical cell (PEC) for H_2 production, with an efficiency higher than 10%. Therefore, an improvement in charge generation, separation and transfer at the electrodes is required to enhance the efficiency of the PEC system, which is currently lower than photovoltaic cells coupled to electrolyzers [4].

Semiconductor materials for this kind of approach have been studied extensively since the first report on photo-electrochemical water splitting with TiO_2 by Fujishima and Honda in 1972 [5]. Of all the different kinds of semiconductor materials [6] that are available, metal oxides have attracted a great deal of interest thanks to their cost effectiveness and stability. Among these metal oxide semiconductors, bismuth vanadate has demonstrated to be a promising material for water oxidation [7-9]. $BiVO_4$ presents three crystal systems: a Scheelite structure with monoclinic (s-m) (highly active), tetragonal (s-t) phases, and a zirconia structure with a tetragonal (z-t) phase [8] Some of the commonly quoted advantages of $BiVO_4$ are: (i) a low band gap of about 2.4 eV (for monoclinic scheelite), which roughly corresponds to a 520 nm wavelength that allows a good visible-photon absorbance capability [8, 10]; (ii) a valence band (VB) position which is sufficiently negative (ca. 2.4 V vs RHE) with respect to water oxidation, and a conduction band (CB) that is around 0 V vs. RHE, thus implying a thermodynamic level close to H_2 [8, 10-12]; (iii) the effective masses of the electrons and holes have been estimated to be lower than similar semiconductors (*e.g.* In_2O_3 or TiO_2), and this, in principle, would result in improved separation and extraction processes of the electron-hole pairs [8, 10, 12]; and (iv) it is composed of inexpensive elements and is non-toxic [11, 12].

Although the synthesis of $BiVO_4$ powders is useful for an in-depth analysis of crystal properties, these powders are actually unsuitable from the practical application point of view. For this reason, photoelectrodes are dealt with the development of devices for solar water oxidation. The photoelectrode concept has become popular, compared to the direct utilization of powder, since the compartmentalization of O_2 and H_2 is simpler. Different approaches with diverse performances and efficiencies have been applied to date. In general, the formation of a thin film over a conductive substrate, usually fluorine doped tin oxide (FTO) or the more expensive indium tin oxide (ITO), is achieved via a solution-based method [13], electrochemical deposition [14], direct crystal growth [15], or powder synthesis (as described above) and later impregnation of these as films [16].

Among the available in situ thin film deposition techniques, dip coating has attracted a great deal of attention because of its advantages. Dip coating is in fact a simple method of depositing a uniform liquid thin film which then solidifies into a coating on a substrate [13]. Many reports have been written on the fabrication of thin $BiVO_4$ films by the available techniques [8, 14, 17, 18], but there is still an urgent need to address the importance of the thickness of $BiVO_4$ films and their characteristics regarding the photocatalytic activity of the system.

The simple fabrication of stable and reproducible thin films of pure $BiVO_4$ on FTO conducting glass electrodes, employing a dip coating procedure, and their use as photoanodes for the water oxidation reaction are herein reported. Insights are provided, from electrochemical impedance spectroscopy, about the different types of processes that occur in the film as a function of the thickness of the as synthesized $BiVO_4$ film. In particular, the quantification of the different charge transfer and transport mechanisms, namely the electrolyte-electrode charge transfer as well as the charge transport inside the bismuth vanadate film, has been done in the perspective of capturing the rate determining steps of the water oxidation half-reaction, at the different operating conditions here investigated. These images have

Applied Catalysis A: General xxx (2015) xxx–xxx
DOI: 10.1016/j.apcata.2015.01.019

clearly pointed out that the thickness of the film is a key factor for the performance of the catalyst.

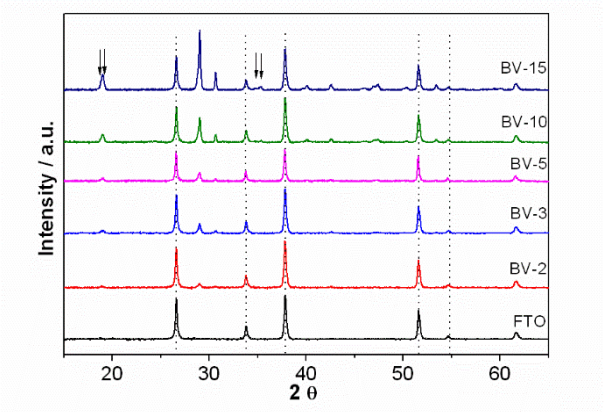

Fig. 1. XRD spetra of the $BiVO_4$ films for different numbers of dip-coated layers.

2. Experimental section

2.1. Materials

Bismuth (III) nitrate pentahydrate ($Bi(NO_3)_3 \cdot 5H_2O$), ammonium metavanadate (NH_4VO_3) and nitric acid (HNO_3) were purchased from Sigma Aldrich. The conductive FTO glasses, with a sheet resistance of 7 $\Omega.cm^{-2}$, were obtained from Solaronix Inc.

2.2. Synthesis of thin $BiVO_4$ films

The raw materials involved in this process are bismuth nitrate, ammonium metavanadate and nitric acid. 1.121 g of $Bi(NO_3)_3.5H_2O$ and 0.292 g of NH_4VO_3 were mixed in 50 ml of 1M HNO_3 until a clear homogenous solution was obtained. The solution was then filtered through Whatman filter paper to obtain a clear solution. This solution was employed in the dip coating procedure. The FTO electrodes were cleaned in acetone, ethanol and then with distilled water using an ultrasound bath. The dip coating process was performed at a controlled speed of $1mms^{-1}$. A series of electrodes with different thicknesses was prepared by varying the number of layers through the dip-coating procedure. Thereafter, each sample is designated as BV-*n*, where *n* stands for the number of deposited layers. A calcination step was performed at 450 °C for 20 min in air after each dipping. A final calcination was performed on all of the samples at 450 °C for 2 h in air.

2.2. Characterization

The $BiVO_4$ samples were characterized through X-ray

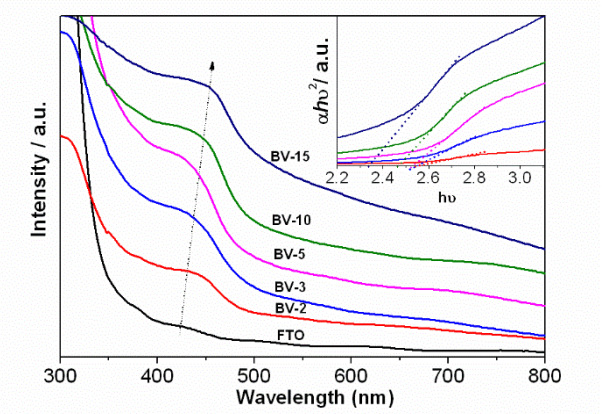

Fig. 2. UV-vis diffuse reflectance spectra of the $BiVO_4$ films for different numbers of dip-coated layers. Inset: Tauc plots of the same films.

diffraction (XRD) using an X'Pert Phillips diffractometer equipped with Cu K_α radiation (λ = 1.5418 Å) at 40 kV and 30 mA. All the patterns were recorded in the 5 – 60 ° range, with a step size of 0.02 °. The crystallite sizes of the samples were estimated using the Scherrer formula [13, 19]:

$$D = \frac{K\lambda}{\beta cos\theta} \quad (1)$$

where D is the average crystallite size (nm), λ is the wavelength of the X-ray radiation, K is the shape factor (0.9), β is the peak width at half-maximum height, corrected for instrumental broadening, and 2θ = 30.6 °. The UV-vis diffuse reflectance spectra were recorded on a UV-Vis Varian Cary 5000 spectrophotometer equipped with an integrating sphere. The morphology of the samples was investigated by means of scanning electron microscopy (SEM) using a FE-SEM MERLIN ZEISS equipped with an energy dispersive analysis system (EDS), which was employed to obtain an insight into the bulk element composition of the sample.

2.2. Photo-electrochemical characterization

The photoelectrochemical characterizations of the $BiVO_4$ electrodes used as photoanodes for the water oxidation reaction were carried out in an aqueous 0.1M Na_2SO_4 electrolyte solution (pH ~ 6.2), employing a multi-channel VSP potentiostat/galvanostat made by BioLogic. A three-electrode system, consisting of the

$BiVO_4$ material as the working electrode, a platinum counter electrode and an Ag/AgCl (3M) as the reference electrode was used. Linear scan voltammetries (LSVs) were performed in the dark and under simulated solar light, using a 450 W Xe lamp by Newport with an AM 1.5 filter and a water filter. The intensity of the light was maintained at 100 mW cm^{-2} by adjusting the distance between the source and the PEC. Chrono-amperometry (*I-t*) measurements were performed at 0.6 V vs. Ag/AgCl over continuous light on-off cycles. Electrochemical Impedance Spectroscopy (EIS) measurements were conducted in the 100 mHz to 1MHz frequency range, with an amplitude of 25 mV, under different applied DC potentials in the -0.3 to 0.9 V vs. Ag/AgCl range, with 0.3 V steps. The EIS data were modeled using ZSimpWin (EChemSoftware). Incident-photon-to-current-efficiency (IPCE) was recorded using a Newport Xe lamp (150 W) coupled to a monochromator (Cornestone 130 by Newport), by varying the wavelength of the incident light from 300 nm to 570 nm (step size: 10 nm), at an applied potential of 0.6 V vs. Ag/AgCl. The electrochemical data presented in the work refer to the reversible hydrogen electrode (RHE) potential, calculated with $E_{RHE} = E_{Ag/AgCl} + 0.209\ V + 0.059 \cdot pH$.

3. Results and discussions

3.1. Structural, morphological and optical investigations

Prior to being used as photoanodes for the water splitting reaction, $BiVO_4$ films of various thickness were characterized through different techniques, such as XRD, UV-vis spectroscopy, SEM and EDS.

The XRD analysis has confirmed that all the films exhibit the monoclinic phase of $BiVO_4$ (which is considered as the only active phase). The tetragonal zircon-type phase in fact changes to a monoclinic scheelite-type phase after calcining at temperatures higher than 400 °C [20]. It can be seen from Fig. 1 that, regardless of the number of deposited layers, the patterns of the diverse samples present the same typical peaks as the monoclinic family of $BiVO_4$ (standard card No. 14-0688, space group: *I2/a*, a = 5.195, b = 11.701, c = 5.092, β = 90.38 °). The monoclinic nature of $BiVO_4$ can be confirmed from the peak splitting that is observed at 18.5 ° and 35 ° of 2θ, which is indicated with arrows over the peaks. The intensity of the $BiVO_4$ peaks grows as the number of layers is increased, which indicates that a larger amount of material is deposited onto the FTO surface. In addition, the crystal sizes were also determined using the Scherrer equation, as stated in Eq. (1), and are reported in Table 1. By observing these values, it can be concluded that the crystallite size increases as the number of deposited layers is incremented, probably due to the increased amount of material and the larger number of intermediate calcination steps performed at 450 °C for 20 min.

To calculate the electronic states of the semiconductor materials, diffuse reflectance spectra (DRS) were used. Fig. 2 shows the UV-Vis reflectance spectra of the films, as well as that of the FTO substrate. The Tauc plots, which give indications on the band gap of the material, are reported in the inset. All the samples show absorption in the visible region of the electromagnetic spectrum. This gives information about the monoclinic nature of the $BiVO_4$ samples [21]. Changes in the absorption edges can be recognized among the $BiVO_4$ samples along with the FTO substrate. In particular, a red shift was observed when the thickness of the film was increased. The band gaps were calculated using the Tauc plot and are reported in Table 1. A reduction in the band gap can be observed for an increase in the thickness and crystallite size of the $BiVO_4$. As in our previous work [9], this could be explained by a higher delocalization of the electron and hole pairs and a greater overlapping between the Bi 6s and O 2p orbitals with an increase in $BiVO_4$ crystals. The morphologies of the deposited $BiVO_4$ films were studied through FESEM analysis. A considerable difference in the samples can be observed from an examination of the top view in Fig. 3 (a, b and c). Some pores in fact form during the calcination process as the solvent evaporates and the particles start to agglomerate. This could facilitate the penetration of light and electrolyte through the film. In addition, the thicknesses of the samples were determined by means of FESEM (see Fig. 3d), and the values are reported in Table 1. As expected, the larger the number of deposited layers, the higher the film thickness. A maximum of 210 nm was obtained after 15 repeated

Applied Catalysis A: General xxx (2015) xxx–xxx
DOI: 10.1016/j.apcata.2015.01.019

deposition steps. The atomic and weight percentages of bismuth and vanadium were acquired from EDS

Applied Catalysis A: General xxx (2015) xxx–xxx
DOI: 10.1016/j.apcata.2015.01.019

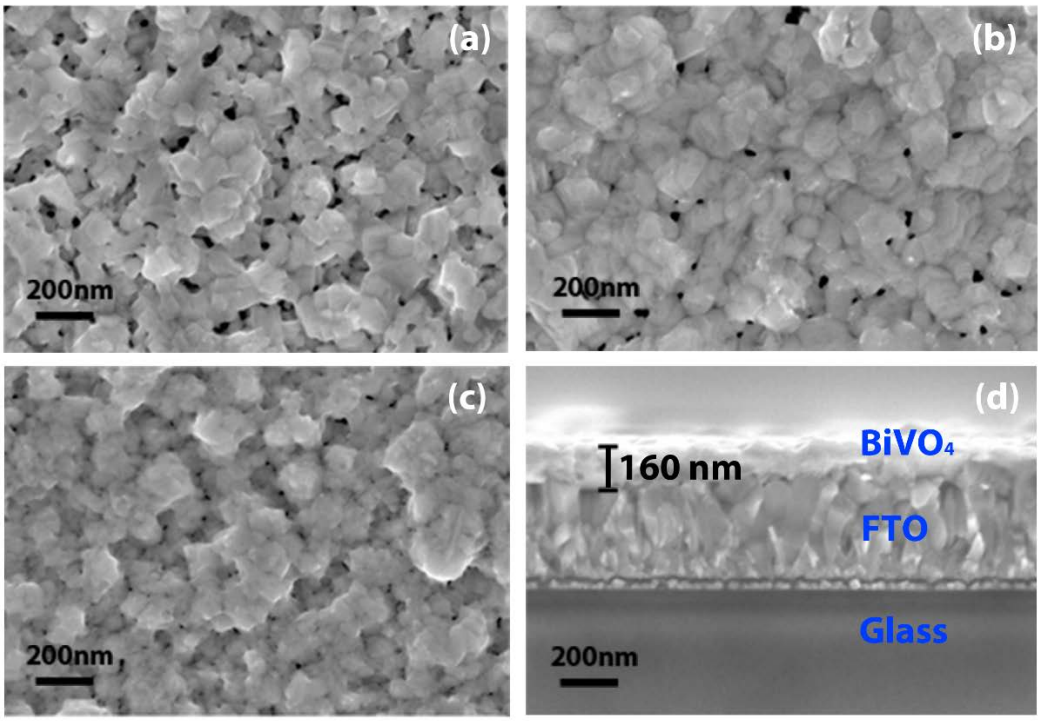

Fig. 3. FESEM images of the $BiVO_4$ films: top view of the BV-3 (a), BV-10 (b) and BV-15 (c) samples, cross section of the BV-10 sample with measurement of the $BiVO_4$ film thickness.

Table 1. Properties of the $BiVO_4$ films as a function of the number of coated layers

Sample	Bi / atomic %	V / atomic %	Thickness / nm	Crystallite size / nm	Band gap / eV
BV-2	0.65	1.28	60	24	2.55
BV-3	0.97	1.93	80	28	2.51
BV-5	1.86	2.90	115	34	2.50
BV-10	4.06	5.29	160	52	2.46
BV-15	6.79	7.60	210	65	2.35

analysis and are presented in Table 1. These percentages offer further confirmation of the increase in the amount of $BiVO_4$ material on the FTO electrode and of the purity of the material up to a certain extent. Moreover, the EDS analysis results reflect the different "surface to bulk ratio" of the different $BiVO_4$ films. Since the V/Bi ratio is different in the surface and in the bulk, thinner films result in a value more representative of the film surface, while thicker films show values approaching 1, which is the stoichiometric value in $BiVO_4$.

3.2. Photocatalytic performance

The photocatalytic activity of the $BiVO_4$ films was evaluated by using them as anodes for the photo-electrochemical water splitting reaction. The LSV curves of the photoelectrodes acquired under AM1.5G illumination (see Fig. 4a) show the current density as a function of the applied potential in the PEC system. The current density remains negligible for all the samples until the water oxidation onset potential is reached: this potential represents the thermodynamic limit value, beyond which water electrolysis occurs. It is worth noting that all the curves are characterized by an onset potential well below 1.23 V, which represents the minimum voltage that should be applied to obtain cold water dissociation in dark conditions [6, 22]: this feature highlights the photocatalytic activity of the fabricated films. As can be observed from all the curves in Fig. 4a, the current increases quite linearly without any disturbances and this indicates that the material is not undergoing any changes. The effect of the photoanode thickness on the catalytic activity is also visible in the LSV curves. Thinner films are characterized by a rising current density while the number of deposited layers increases. The maximum photocatalytic activity was reached for the 10-layer

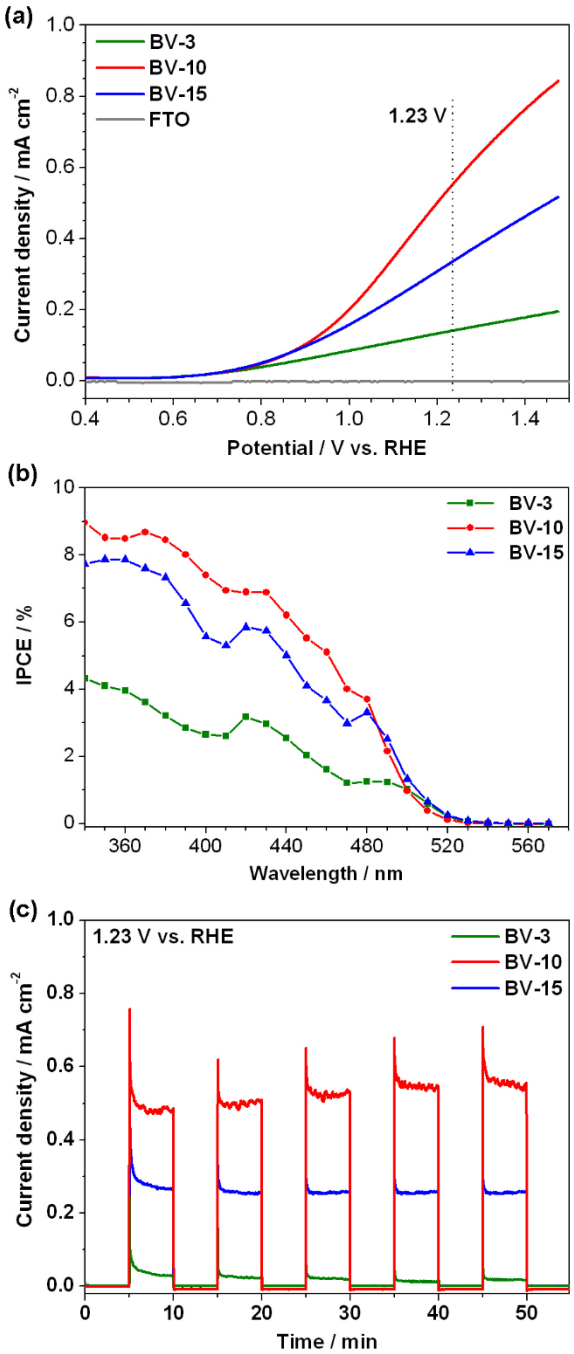

Fig. 4. Photo-electrochemical characterization of the $BiVO_4$ electrodes with different thicknesses: (a) Photocurrent response vs. potential under simulated sunlight illumination (AM 1.5G, 100 mW cm^{-2}), (b) IPCE spectra, and (c) crono-amperometric curves at 1.23 V vs. RHE, under continuous dark-light (AM 1.5G, 100 mW cm^{-2}) cycles.

sample, while the thickest film exhibited a lower current.

The behavior of the $BiVO_4$ films' photo-activity reflects the conclusions that were drawn in [9] from powder-form catalysts: the water oxidation activity is inversely correlated to the band gap and directly related to the crystalline size of the powder samples, as also observed in the current work. This mutual correlation could be due to two possible phenomena: the first is directly linked to a potential loss of symmetry constraint in the smaller crystallites, which leads to a smaller contribution of the Bi 6s overlapping with O 2p due to the lone-pair distortion and ultimately to widening of the transition band gap. The second could be connected to the quantum-size phenomena, in which nanosized semiconductor particles exhibit a remarkable change in their absorption spectra due to their reduction in size, in comparison to the bulk materials [23]; Kho et al. [24] attributed this quantization effect to the higher than normal $BiVO_4$ band gap in particles of <100 nm. These occurrences were indeed observed in Table 1, where a smaller crystallite size was correlated to a higher band gap. In addition to this, the interconnection among particles of subsequent deposited layers is highly important, since grains defects could induce a higher charge carriers recombination and an overall lower activity, as discussed later for the thicker films, i.e. BV-15.

The same feature is also evident in the results of the IPCE measurements (Fig. 4b): the total photocurrent of the BV-10 film is larger than those of the thinner (BV-3) and thicker (BV-15) films. However, the IPCE spectrum of all the samples exhibits non-zero values for lower wavelengths than 530 nm, thus confirming that $BiVO_4$ films are efficient catalytic materials for solar-driven oxidation reactions.

Similarly, the chrono-amperometric measurements, which were performed in order to check the stability of the $BiVO_4$ photoanodes, have also revealed that the current density dependence on the thickness of the material is not monotonic (see Fig. 4c). In fact, even though the *I-t* curves show good photocurrent stability under numerous light on-off cycles over a longer period than 60 min, some limiting parameters emerge for thicker films, and show a negative influence on the activity. The charge transfer mechanism that occurs in thin $BiVO_4$ films was analyzed in detail by means of the electrochemical impedance spectroscopy technique in order to obtain a better understanding of this kind of behavior, as reported in the following section.

Applied Catalysis A: General xxx (2015) xxx–xxx
DOI: 10.1016/j.apcata.2015.01.019

3.3. Electrochemical impedance spectroscopy analysis

EIS is a well known technique that is widely employed in electrochemical systems and devices for different kinds of applications [23], including photo-electrochemical water splitting [24]. Here it has been exploited to study the charge transfer process at the semiconductor/electrolyte interface and the charge transport inside the catalyst. Examples of the results are reported in Fig. 5. A decrease in the total impedance for an increase in the applied potential is evident in the Bode plot of modulus related to the BV-10 sample, in agreement with the results obtained from LSV analysis. Looking at the phase spectrum, two processes can be recognized for low applied potentials, namely the charge transfer at the solid/liquid interface (Helmholtz layer), which can be identified in the low frequency region, and the charge transport inside the film (depletion layer), which is distinguishable in the high frequency region [25]. The charge transfer becomes faster as the voltage increases (i.e. the corresponding peak shift toward higher frequencies), and is finally comparable with that of the other process for potentials larger than 0.6 V vs. Ag/AgCl (corresponding to the onset potential in Fig. 4a). At these potentials it is no more possible to distinguish the kinetics of the two processes by the impedance technique. However, being the charge transfer the slower process, it is possible to state that it represents the controlling step of the water oxidation half-reaction.

The Bode plots of the impedance of the $BiVO_4$ electrodes with different thicknesses, acquired under illumination at 0.9 V vs. Ag/AgCl, are reported in Fig. 6. The modulus of the BV-3 sample is characterized by a larger impedance than the other two films, thus showing that a minor current is produced during the electrolysis reaction as a consequence of the reduced quantity of the deposited material. Conversely, the impedance of the thicker film is comparable with that of the BV-10 one. This behavior can be explained by examining the phase plots: the BV-15 sample is in fact characterized by an additional process that occurs at very large frequencies (around 5 kHz), as can be seen from the side feature that is visible in the main peak. A

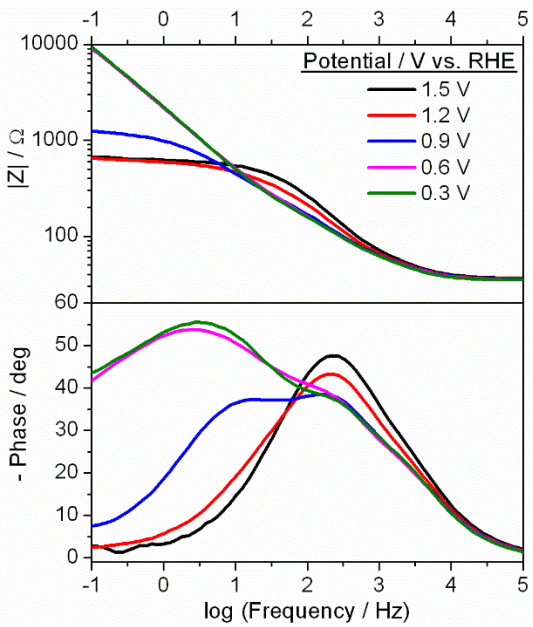

Fig. 5. Bode plots of the EIS measurements in the BV-10 electrode at different applied potentials, under AM 1.5G light illumination (100 mW cm^{-2}).

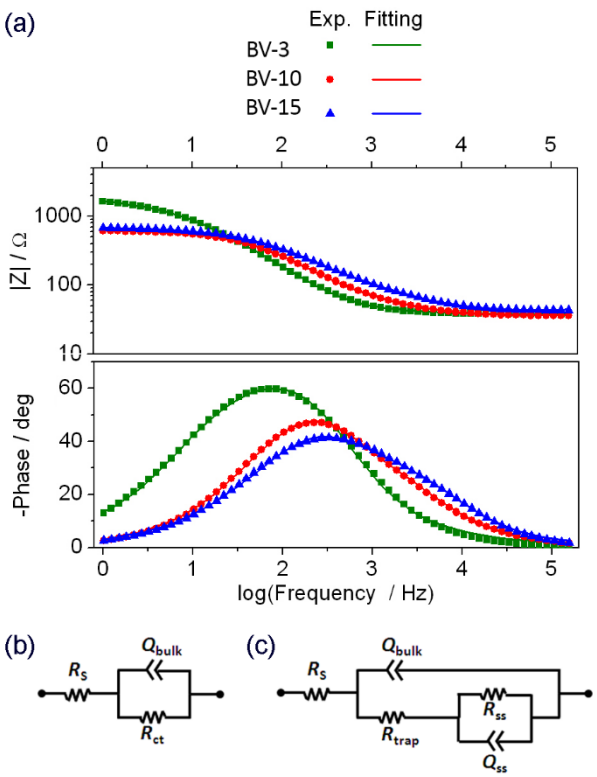

Fig. 6. Bode plots of the EIS measurements (symbols) and fitted data (lines) acquired using the $BiVO_4$ electrodes with different thicknesses at 0.9V vs. Ag/AgCl (1.5 V vs. RHE) under AM 1.5G light tillumination (100 mW cm^{-2}). The experimental data of the BV-3 and BV-10 electrodes were fitted using the equivalent circuit (EC) depicted in (b), while the EC in (c) was employed for the BV-15 electrode.

possible interpretation of this fact is that the charge transfer mechanism has occurred via surface states [26, 27], which could be due to an imperfect interconnection between adjacent layers in the thicker films. On the other hand, the thinner films (up to 10 layers) are characterized by a single charge transfer process.

For this reason, two different equivalent circuits (ECs) were employed to fit the experimental EIS data: the one reported in Fig. 6b for thinner electrodes and the EC shown in Fig. 6c for the BV-15 film. The simpler circuit is constituted by the series resistance R_s (which accounts for the resistances of: the FTO film, the external electrical contacts and the liquid electrolyte) and by the parallel between the charge transfer resistance R_{ct} and the constant phase element (CPE) Q_{bulk}, which represents the direct charge transfer at the semiconductor/electrolyte interface. CPEs were used instead of common capacitance to take into account the frequency dispersion due to the porosity of the films [23, 28]. In the EC in Fig. 6c, R_{ct} is substituted by the resistance R_{trap} (which represents the trapping of charges in the surface states) and by the parallel between the resistance R_{ss} (which models the charge transfer between the electrolyte and the surface states) and the surface state CPE Q_{ss} [26]. The results of the fitting procedures are reported in Fig. 6a, where they are superimposed onto the experimental curves. The R_s values do not depend on the film thickness, as all the values are around 40 Ω. Conversely, the charge transfer resistances was reduced by increasing the number of deposited layers, reaching a minimum of 590 Ω for the BV-10 sample. Hence, the thinnest film (BV-3) has a larger impedance because, although a shorter distance should be traveled by the electrons in the film, the controlling resistance is at the film-electrolyte interface. The lower number of sites involved in the photo-generation of charges (as seen from the UV-vis and IPCE tests) entails a lower rate of charge generation, and thus a higher resistance associated to this step.

The same behavior is exhibited by the charge transfer time, τ_{ct}, calculated through the formula [29]:

$$\tau_{ct} = (R_{ct}Q_{bulk})^{1/n_{ct}} \qquad (2)$$

where n_{ct} is the CPE index: this value is equal to 24 ms for the BV-3 film and reduces to 4 ms for the BV-10 film, thus evidencing a faster process as a consequence of the larger quantity of active material available for the water splitting reaction. As far as the BV-15 sample is concerned, the charge transfer (which occurs through the surface states) shows a time constant comparable with that of the BV-10 film (equal to 2.5 ms), but the presence of the additional trap resistance (equal to 44 Ω) leads to a reduced total catalytic activity compared to the sample grown with 10 deposited layers. This additional resistance corresponds to a higher charge recombination on such trap states, which in turn is observed as a decrease in the total photocurrent (i.e. photocatalytic activity) compared to the sample BV-10. The plots in Figure 6 show this resistance difference between BV-10 and BV-15, referred to the transport of charges within the film, at intermediate frequencies. It is visible that a higher resistance (Fig. 6a, modulus) is referred to the BV-15 curve, coupled to a capacitance effect (Fig. 6a, phase) corresponding to a flank in the phase shift curve's right-hand side.

Conclusions

The photocatalytic activity of $BiVO_4$ has been assessed through the photoinduced oxidation of water. Linear scan voltammetries and chrono-amperometry measurements have been carried out to obtain insights into the activity and stability of the fabricated thin films. It has been revealed that an optimal thickness, which is necessary to obtain the maximum photocatalytic activity of pure $BiVO_4$ thin films, can be obtained.

EIS analysis have been conducted by employing proper equivalent circuits in order to understand the charge transfer and transport processes occurring for different film thicknesses. It has been observed that the increase in the number of coated layers causes the formation of trap states in the thicker films (of about 210 nm), probably due to film imperfections arising from several deposition-calcination cycles. This hinders the charge transfer process at the electrode-electrolyte interphase, being this the main reason for the decrease in the photocatalytic activity of the whole system. Hence, the analysis here presented is of high significance to isolate the rate determining step of the

water oxidation half-reaction, in the perspective of an optimization of $BiVO_4$ photo-electrodes.

Acknowledgments

The financial support from the European Commission on the 7th Framework Program (NMP-2012 Project Eco^2CO_2 No.309701 and FCH-JU Call 2011-1 Project ArtipHyction No. 303435) is gratefully acknowledged.

References

[1] T. Bak, J. Nowotny, M. Rekas, C.C. Sorrell, Photo-electrochemical hydrogen generation from water using solar energy. Materials-related aspects, International Journal of Hydrogen Energy, 27 (2002) 991-1022.
[2] Z. Li, W. Luo, M. Zhang, J. Feng, Z. Zou, Photoelectrochemical cells for solar hydrogen production: current state of promising photoelectrodes, methods to improve their properties, and outlook, Energy & Environmental Science, 6 (2013) 347-370.
[3] M.W. Kanan, D.G. Nocera, In Situ Formation of an Oxygen-Evolving Catalyst in Neutral Water Containing Phosphate and Co^{2+}, Science, 321 (2008) 1072-1075.
[4] M. Gratzel, Photoelectrochemical cells, Nature, 414 (2001) 338-344.
[5] A. Fujishima, K. Honda, Electrochemical photolysis of water at a semiconductor electrode, Nature, 238 (1972) 37-38.
[6] A. Kudo, Y. Miseki, Heterogeneous photocatalyst materials for water splitting, Chemical Society Reviews, 38 (2009) 253-278.
[7] A. Kudo, K. Ueda, H. Kato, I. Mikami, Photocatalytic O_2 evolution under visible light irradiation on $BiVO_4$ in aqueous $AgNO_3$ solution, Catalysis Letters, 53 (1998) 229-230.
[8] Y. Park, K.J. McDonald, K.-S. Choi, Progress in bismuth vanadate photoanodes for use in solar water oxidation, Chemical Society Reviews, 42 (2013) 2321-2337.
[9] S.M. Thalluri, C. Martinez Suarez, M. Hussain, S. Hernandez, A. Virga, G. Saracco, N. Russo, Evaluation of the Parameters Affecting the Visible-Light-Induced Photocatalytic Activity of Monoclinic $BiVO_4$ for Water Oxidation, Industrial & Engineering Chemistry Research, 52 (2013) 17414-17418.
[10] A. Walsh, Y. Yan, M.N. Huda, M.M. Al-Jassim, S.-H. Wei, Band Edge Electronic Structure of $BiVO_4$: Elucidating the Role of the Bi s and V d Orbitals, Chemistry of Materials, 21 (2009) 547-551.
[11] K. Maeda, Photocatalytic water splitting using semiconductor particles: History and recent developments, Journal of Photochemistry and Photobiology C: Photochemistry Reviews, 12 (2011) 237-268.
[12] Z. Zhao, Z. Li, Z. Zou, Electronic structure and optical properties of monoclinic clinobisvanite $BiVO_4$, Physical Chemistry Chemical Physics, 13 (2011) 4746-4753.
[13] Q. Jia, K. Iwashina, A. Kudo, Facile fabrication of an efficient $BiVO_4$ thin film electrode for water splitting under visible light irradiation, Proceedings of the National Academy of Sciences, 109 (2012) 11564-11569.
[14] R. Saito, Y. Miseki, K. Sayama, Highly efficient photoelectrochemical water splitting using a thin film photoanode of $BiVO_4/SnO_2/WO_3$ multi-composite in a carbonate electrolyte, Chemical Communications, 48 (2012) 3833-3835.
[15] J. Su, L. Guo, S. Yoriya, C.A. Grimes, Aqueous Growth of Pyramidal-Shaped $BiVO_4$ Nanowire Arrays and Structural Characterization: Application to Photoelectrochemical Water Splitting, Crystal Growth & Design, 10 (2009) 856-861.
[16] K.P.S. Parmar, H.J. Kang, A. Bist, P. Dua, J.S. Jang, J.S. Lee, Photocatalytic and Photoelectrochemical Water Oxidation over Metal-Doped Monoclinic BiVO4 Photoanodes, ChemSusChem, 5 (2012) 1926-1934.
[17] S.J. Hong, S. Lee, J.S. Jang, J.S. Lee, Heterojunction $BiVO_4/WO_3$ electrodes for enhanced photoactivity of water oxidation, Energy & Environmental Science, 4 (2011) 1781-1787.
[18] F.F. Abdi, L. Han, A.H.M. Smets, M. Zeman, B. Dam, R. van de Krol, Efficient solar water splitting by enhanced charge separation in a bismuth vanadate-silicon tandem photoelectrode, Nat Commun, 4 (2013) Article nr. 2195.
[19] D. Grosso, How to exploit the full potential of the dip-coating process to better control film formation, Journal of Materials Chemistry, 21 (2011) 17033-17038.
[20] H. Fan, T. Jiang, H. Li, D. Wang, L. Wang, J. Zhai, D. He, P. Wang, T. Xie, Effect of $BiVO_4$ Crystalline Phases on the Photoinduced Carriers Behavior and Photocatalytic Activity, The Journal of Physical Chemistry C, 116 (2011) 2425-2430.
[21] S.M. Thalluri, C. Martinez Suarez, S. Hernández, S. Bensaid, G. Saracco, N. Russo, Elucidation of important parameters of $BiVO_4$ responsible for photo-catalytic O_2 evolution and insights about the rate of the catalytic process, Chemical Engineering Journal, 245 (2014) 124-132.
[22] J.Y. Kim, G. Magesh, D.H. Youn, J.-W. Jang, J. Kubota, K. Domen, J.S. Lee, Single-crystalline, wormlike hematite photoanodes for efficient solar water splitting, Sci. Rep., 3 (2013).
[23] X. Dominguez-Benetton, S. Sevda, K. Vanbroekhoven, D. Pant, The accurate use of impedance analysis for the study of microbial electrochemical systems, Chemical Society Reviews, 41 (2012) 7228-7246.
[24] T. Lopes, L. Andrade, H.A. Ribeiro, A. Mendes, Characterization of photoelectrochemical cells for water splitting by electrochemical impedance spectroscopy, International Journal of Hydrogen Energy, 35 (2010) 11601-11608.
[25] D. Hidalgo, R. Messina, A. Sacco, D. Manfredi, S. Vankova, E. Garrone, G. Saracco, S. Hernández, Thick mesoporous TiO_2 films through a sol–gel method involving a non-ionic surfactant: Characterization and enhanced performance for water photo-electrolysis, International Journal of Hydrogen Energy, 39 (2014) 21512–21522.
[26] B. Klahr, S. Gimenez, F. Fabregat-Santiago, T. Hamann, J. Bisquert, Water Oxidation at Hematite Photoelectrodes: The Role of Surface States, Journal of the American Chemical Society, 134 (2012) 4294-4302.
[27] L. Badia-Bou, E. Mas-Marza, P. Rodenas, E.M. Barea, F. Fabregat-Santiago, S. Gimenez, E. Peris, J. Bisquert, Water Oxidation at Hematite Photoelectrodes with an Iridium-Based

Catalyst, The Journal of Physical Chemistry C, 117 (2013) 3826-3833.

[28] J. Bisquert, G. Garcia-Belmonte, F. Fabregat-Santiago, N.S. Ferriols, P. Bogdanoff, E.C. Pereira, Doubling Exponent Models for the Analysis of Porous Film Electrodes by Impedance. Relaxation of TiO_2 Nanoporous in Aqueous Solution, The Journal of Physical Chemistry B, 104 (2000) 2287-2298.

[29] S. Hernández, M. Tortello, A. Sacco, M. Quaglio, T. Meyer, S. Bianco, G. Saracco, C.F. Pirri, E. Tresso, New Transparent Laser-Drilled Fluorine-doped Tin Oxide covered Quartz Electrodes for Photo-Electrochemical Water Splitting, Electrochimica Acta, 131 (2014) 184-194.